Research Paper
J. Astron. Space Sci. 36(3), 105-113 (2019)
https://doi.org/10.5140/JASS.2019.36.3.105

JASS Journal of Astronomy and Space Sciences

The Barium Star HD204075: Iron Abundance and the Absence of Evidence for Accretion

Yeuncheol Jeong[1], Alexander Yushchenko[2†], Vira Gopka[3], Volodymyr Yushchenko[3], Pakakaew Rittipruk[4], Kyung Sook Jeong[1], Aizat Demessinova[5]

[1]Daeyang Humanity College, Sejong University, Seoul 05006, Korea
[2]Astrocamp Contents Research Institute, Goyang 10329, Korea
[3]Astronomical Observatory, Odessa National University, Odessa 65014, Ukraine
[4]Department of Physics and Astronomy, Sejong University, Seoul 05006, Korea
[5]Physico-Technical Department, Al Farabi Kazakh National University, Almaty 050040, Kazakhstan

Spectroscopic observations of barium star ζ Capricornus (HD204075) obtained at the 8.2 m telescope of the European Southern Observatory, with a spectral resolving power R = 80,000 and signal to noise ratio greater than 300, were used to refine the atmospheric parameters. We found new values for effective temperature (T_{eff} = 5,300 ± 50 K), surface gravity (log g = 1.82 ± 0.15), micro-turbulent velocity (υ_{micro} = 2.52 ± 0.10 km/s), and iron abundance (log N (Fe) = 7.32 ± 0.06). Previously published abundances of chemical elements in the atmosphere of HD204075 were analyzed and no correlations of these abundances with the second ionization potentials of these elements were found. This excludes the possible influence of accretion of hydrogen and helium atoms from the interstellar or circumstellar environment to the atmosphere of this star. The accretion of nuclear processed matter from the evolved binary companion was primary cause of the abundance anomalies. The young age of HD204075 allows an estimation of the time-scale for the creation of the abundance anomalies arising from accretion of interstellar hydrogen and helium as is the case of stars with low magnetic fields; which we estimate should exceed 10^8 years.

Keywords: barium star, star (HD204075), star abundance, star accretion, chemically peculiar star

1. INTRODUCTION

In this paper we refine the atmospheric parameters and atmospheric iron abundance of the main component of barium star HD204075 (ζ Capricornus), using high quality spectral observations, modern software and updated atomic line databases. We analyzed previously published abundances of chemical elements in the main component of this barium star (Antipova et al. 2004; Gopka et al. 2006) to examine the possibility of hydrogen and helium accretion from the interstellar environment.

The reactions of hydrogen atoms with the first ions of chemical elements in the atmospheres of metallic-line stars was first proposed by Greenstein (1949) as an explanation for observed underabundances of elements with second ionization potentials close to the ionization potential of hydrogen (13.6 eV), detected in the atmospheres of these stars. Greenstein (1949) explained the underabundances by charge-exchange reactions between the first ions of these elements and hydrogen atoms in stellar atmospheres. As a result of these reactions, the first ions of these elements lose one more electron, become the second ions, and, after obtaining a great enough kinetic energy, are pushed out of the photosphere, creating the observed deficiency.

Greenstein (1949) proposed that charge-exchange reactions can have a resonance for elements with second ionization potentials close to 13.6 eV. This explains why these elements should be effectively deleted from the

Received 20 MAY 2019 **Revised** 15 AUG 2019 **Accepted** 16 AUG 2019
†**Corresponding Author**
Tel: +82-2-3408-3567, E-mail: avyushchenko@gmail.com
ORCID: https://orcid.org/0000-0002-9325-5840

photosphere and their abundances (relative to solar) can be significantly lower than the abundances (relative to solar) of other chemical elements whose second ionization potentials are not close to the resonance value. Greenstein (1949) found a decrease of abundance for elements with second ionization potentials between 12 and 16 eV and estimated the width of the resonance to be of the order of 4 eV.

If energy transfer in the photosphere is mostly radiative, any type of anomaly can remain for a long time (Michaud 1970). When energy transfer is mostly convective, any anomalies of chemical abundances in the photosphere should quickly disappear. The barium star HD204075 is a red giant and exhibits mostly radiative energy transfer. Consequently, long-term maintenance of any changes in chemical composition of its photosphere is to be expected.

Havnes (1970, 1971) proposed that hydrogen atoms can accrete from the interstellar environment and this pushes the first ions with proper second ionization potential not only out of the photosphere, but also out of the star. These ions can also decrease the rotational energy of the star and can significantly increase the period of stellar rotation. These charge-exchange reactions were also noted as a possible mechanism for the production of low energy (energies less than 200 MeV/nucleon) galactic cosmic rays. Böhm-Vitense (2006) observed evidence of this effect not only for hydrogen but also helium. She found the under-abundances of chemical elements with second ionization potentials close to the first ionization potential of helium (24.6 eV). Yushchenko et al. (2015) reviewed the features of this phenomenon for B-F type single stars and Jeong et al. (2018) reviewed them for barium type stellar binaries.

Yushchenko et al. (2015) and Jeong et al. (2018) used the published abundances for usual stars with low magnetic fields and detected this phenomenon for all objects, including objects located in regions with a low density of interstellar matter. Consequently, we expect that under-abundances can be a result of the interaction of a stellar photosphere with low density interstellar matter, with the duration of such interaction being in the order of the star's life time. Even weak magnetic fields can be sufficient for producing anomalous chemical compositions over long time intervals. It is important to establish the lower limit of this time interval and we provide an estimate here.

This type of accretion manifests itself in the correlations between the relative abundances of chemical elements and the second ionization potentials of these elements, as compared to solar. The theory of this effect has not been developed in detail in previously published studies.

Proffitt & Michaud (1989) discussed accretion from the evolved components of binary systems in combination with radiative diffusion (Michaud 1970). In contrast to radiative diffusion, the accretion of hydrogen and helium is not widely accepted as a possible explanation of chemical anomalies in stellar atmospheres. The investigation of this accretion in different types of stellar atmospheres will help to develop or to reject the theory proposed by Havnes (1970, 1971) and Havnes & Conti (1971) for stars with strong magnetic fields and possibly extend it for the case of stars with weak magnetic fields.

As part of this study, we used the published abundance patterns of HD204075 to estimate the time limits on the creation of anomalies in chemical abundance, which can be produced by the accretion of hydrogen and helium from the interstellar environment. These are the deficiencies of relative (to solar atmospheric values) abundances of chemical elements with second ionization potentials close to the ionization potentials of hydrogen and helium (13.6 eV and 24.6 eV respectively).

2. THE SPECTRUM USED AND ABUNDANCE ANALYSIS

The high-resolution spectrum of HD204075 was taken from the public archive of the European Southern Observatory (Bagnulo et al. 2003). The signal to noise ratio of the spectrum exceeds 300, the resolving power is equal to R = 80,000 and the wavelength coverage ranged from 3,040–10,400 Å. URAN code (Yushchenko 1998) was used to place the continuum, to identify spectral lines and to measure the equivalent width of these lines.

To determine the continuum level and to identify the various lines, the updated version of the suite of codes known as the SYNTHE code, developed by Kurucz in 1993, was used to generate the synthetic spectrum for the whole region of the observed wavelengths. Line data were taken from the, Hirata & Horaguchi (1995) line list, Fuhr & Wises (2006), and the Kurucz (1993), VALD (Piskunov et al. 1995), Morton (2000), and DREAM (Biémont et al. 2002) databases, as well as other sources. The clean and not strongly blended lines in the observed spectrum were selected on the basis of comparisons with synthetic spectrum. Synthetic spectrum was calculated for the whole wavelength region covered by observations. More details about the calculation procedure can be found in Yushchenko et al. (2015) and Kang et al. (2012, 2013).

To find the effective temperature, surface gravity, metallicity, and iron abundance of HD204075, the method developed by Yushchenko et al. (1999) and Gopka et al. (2004), was used. This method uses the iron abundances

calculated for different spectral lines using atmosphere grid models and micro-turbulent velocities. The steps in effective temperature and surface gravity should be selected to be less or equal to the expected precision of the determination of parameters. For each model, calculations of abundance were made with different values of micro-turbulent velocities. Usually the calculations for two grids, constructed using interpolation with different steps in effective temperature and surface gravity, were sufficient. Interpolation was necessary because the grid sizes of atmospheric models were not sufficiently precise.

The analysis of calculations of abundance for a grid of atmospheric models allows selection of the best parameters. The results of the last iteration are shown in Fig. 1. The grid of atmospheric models for this calculation with effective temperatures from T_{eff} = 5,100 K to T_{eff} = 5,400 K (step size 10 K) and surface gravities from log g = 1.5 to log g = 2.0 (step size 0.02) were prepared by interpolation of Kurucz (1993) atmosphere models. A detailed description of methods can be found in Kang et al. (2012, 2013). The true values of effective temperature and surface gravity should be near the intersections of dark edges in panel F of Fig. 1. This region is limited by surface gravities 1.78 < log g < 1.86 and effective temperatures 5,280 K < T_{eff} < 5,320 K. The values T_{eff} = 5,300 ± 50 K and log g = 1.82 ± 0.15 were selected. The pointed errors exceeded the steps of the grid of atmospheric models used in the last iteration and include possible systematic errors.

The best micro-turbulent velocity of the atmosphere model with these parameters was υ_{micro} = 2.52 ± 0.10 km/s, the iron abundance calculated using 105 lines of neutral iron and 31 lines of singly ionized iron was log N (Fe) = 7.32 ± 0.06 (in the scale log N (H) = 12). This iron abundance corresponds to [Fe/H] = –0.18 if the solar iron abundance was set to logN (Fe) = 7.50 (Asplund et al. 2009). Alternatively, [Fe/H] = –0.15 if we accept the solar value logN (Fe) = 7.47 (Scott et al. 2015).

Table 1 shows the list of iron lines used in this study. The first two columns of Table 1 are the wavelength and the line identification; the third through sixth column are the equivalent width, measured in milliangstroms (mÅ); next are the oscillator strength and low level energy, measured in electron-volts (eV); and, finally, the derived abundances, measured in the scale logN (H) = 12. Table 2 compares the parameters of HD204075 main component previously published, and our values.

3. DISCUSSION

Our values of effective temperature, surface gravity, and metallicity are within the typical error boxes of previously published values (Table 2). We will use our values to estimate the homogeneous set of abundances of chemical elements in the atmosphere of HD204075 and to compare

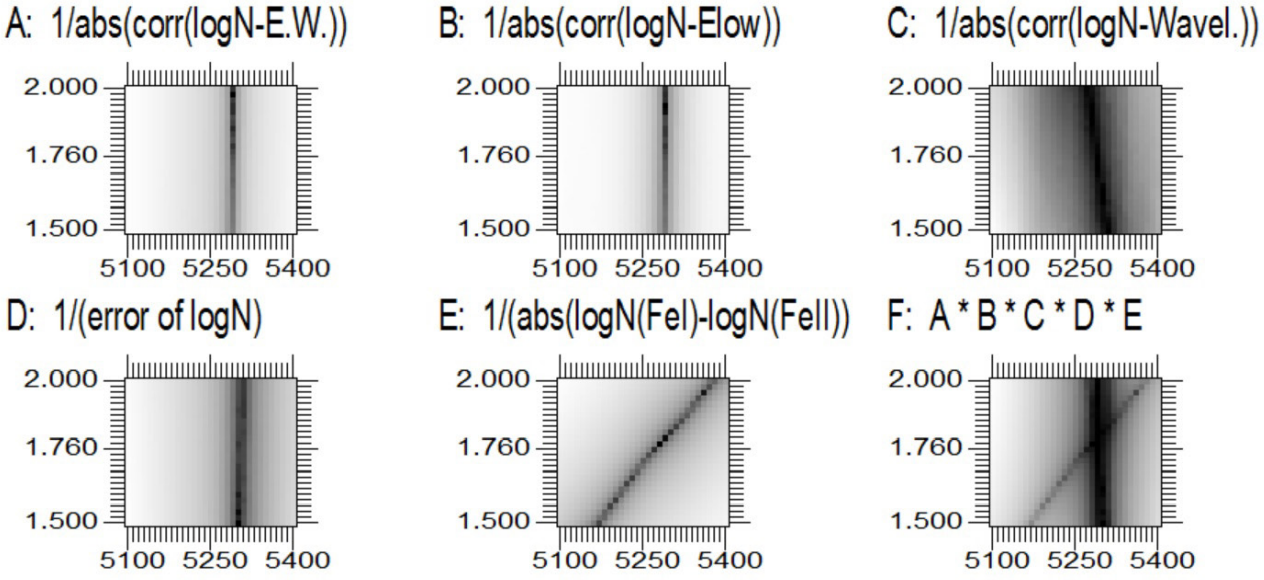

Fig. 1. Determination of atmospheric parameters of HD204075. Panels A–C show the correlation coefficients between the iron abundances found from individual lines of neutral iron and the equivalent widths, the low-level energies, and the wavelengths of these lines, respectively. The darkness of the panels is proportional to the reciprocal values of correlation coefficients. Panel D displays the reciprocal values of errors in mean iron abundance, calculated using the lines of neutral iron. Panel E is the reciprocal values of differences between the iron abundances found using the lines of neutral and ionized iron. Panel F is the multiplication of panels A–E. The axes of each panel are the effective temperatures and the logarithms of surface gravities. Kurucz (1995) grid of atmosphere models with metallicity [Fe/H] = –0.2 was used for these calculations.

Table 1. Iron lines in the spectrum of HD204075

Wavelength (angstroms)	Identification	Eq.Width (miliangstroms)	lggf	E_{low} (eV)	logN (logN(H)=12.00)
5,029.618	Fe I	84.0	-2.05	3.415	7.370
5,196.077	Fe I	107.0	-0.74	4.256	7.271
5,198.711	Fe I	157.0	-2.28	2.223	7.370
5,215.180	Fe I	168.0	-0.93	3.266	7.382
5,217.390	Fe I	151.0	-1.17	3.211	7.284
5,242.491	Fe I	134.0	-0.97	3.634	7.274
5,253.462	Fe I	126.0	-1.60	3.283	7.374
5,288.527	Fe I	94.0	-1.51	3.694	7.244
5,322.041	Fe I	107.0	-2.88	2.278	7.243
5,326.142	Fe I	72.0	-2.07	3.573	7.373
5,364.871	Fe I	163.0	0.23	4.445	7.371
5,365.399	Fe I	125.0	-1.24	3.573	7.314
5,367.466	Fe I	166.0	0.35	4.415	7.267
5,373.709	Fe I	88.0	-0.86	4.473	7.335
5,379.575	Fe I	101.0	-1.51	3.694	7.333
5,389.479	Fe I	120.0	-0.41	4.415	7.304
5,560.212	Fe I	77.0	-1.04	4.434	7.309
5,618.632	Fe I	74.0	-1.31	4.209	7.297
5,636.696	Fe I	37.0	-2.56	3.640	7.427
5,638.262	Fe I	115.0	-0.73	4.220	7.289
5,705.464	Fe I	52.0	-1.60	4.301	7.390
5,717.833	Fe I	88.0	-1.10	4.284	7.346
5,741.848	Fe I	48.0	-1.61	4.256	7.289
5,753.122	Fe I	114.0	-0.69	4.260	7.273
5,852.219	Fe I	56.0	-1.30	4.548	7.397
5,856.088	Fe I	53.0	-1.51	4.294	7.294
5,883.817	Fe I	97.0	-1.31	3.959	7.319
5,905.671	Fe I	80.0	-0.77	4.652	7.289
5,930.173	Fe I	125.0	-0.23	4.652	7.383
5,956.694	Fe I	110.0	-4.61	0.859	7.341
5,976.775	Fe I	100.0	-1.31	3.943	7.331
5,987.066	Fe I	93.0	-0.43	4.795	7.271
6,003.010	Fe I	118.0	-1.12	3.881	7.338
6,007.960	Fe I	90.0	-0.66	4.652	7.305
6,008.554	Fe I	127.0	-0.99	3.883	7.339
6,024.049	Fe I	144.0	0.05	4.548	7.267
6,027.051	Fe I	104.0	-1.06	4.076	7.275
6,065.482	Fe I	194.0	-1.53	2.608	7.409
6,078.491	Fe I	104.0	-0.30	4.795	7.285
6,079.008	Fe I	64.0	-0.95	4.652	7.248
6,127.906	Fe I	72.0	-1.40	4.142	7.258
6,151.617	Fe I	93.0	-3.37	2.176	7.342
6,165.360	Fe I	72.0	-1.55	4.142	7.408
6,173.334	Fe I	129.0	-2.88	2.223	7.373
6,200.313	Fe I	121.0	-2.44	2.608	7.250
6,213.430	Fe I	138.0	-2.66	2.223	7.277
6,219.281	Fe I	157.0	-2.43	2.198	7.277
6,229.226	Fe I	80.0	-2.81	2.845	7.354
6,240.646	Fe I	96.0	-3.23	2.223	7.287
6,252.556	Fe I	192.0	-1.77	2.404	7.352
6,265.132	Fe I	155.0	-2.54	2.176	7.321
6,290.969	Fe I	88.0	-0.61	4.733	7.294
6,322.685	Fe I	125.0	-2.43	2.588	7.255
6,335.330	Fe I	166.0	-2.44	2.198	7.379
6,336.823	Fe I	148.0	-1.05	3.686	7.426
6,411.648	Fe I	164.0	-0.72	3.653	7.292
6,419.949	Fe I	121.0	-0.24	4.733	7.367

Table 1. Continued

Wavelength (angstroms)	Identification	Eq.Width (miliangstroms)	lggf	E_{low} (eV)	logN (logN(H)=12.00)
6,430.845	Fe I	198.0	-2.01	2.176	7.327
6,464.661	Fe I	34.0	-5.44	0.958	7.296
6,475.624	Fe I	101.0	-2.94	2.559	7.409
6,481.870	Fe I	112.0	-2.98	2.278	7.268
6,518.366	Fe I	98.0	-2.52	2.831	7.245
6,608.024	Fe I	36.0	-3.95	2.278	7.278
6,609.110	Fe I	112.0	-2.66	2.559	7.252
6,627.540	Fe I	48.0	-1.45	4.548	7.395
6,725.353	Fe I	35.0	-2.14	4.103	7.407
6,750.152	Fe I	134.0	-2.58	2.424	7.313
6,806.843	Fe I	67.0	-3.10	2.727	7.318
6,810.262	Fe I	68.0	-1.12	4.607	7.378
6,828.592	Fe I	91.0	-0.79	4.638	7.382
6,839.830	Fe I	71.0	-3.34	2.559	7.419
6,857.243	Fe I	43.5	-2.04	4.076	7.405
6,843.655	Fe I	85.0	-0.93	4.548	7.340
6,999.884	Fe I	79.0	-1.39	4.103	7.234
7,219.678	Fe I	71.0	-1.50	4.076	7.203
7,223.658	Fe I	115.0	-2.21	3.017	7.287
7,440.952	Fe I	83.0	-0.68	4.913	7.410
7,491.649	Fe I	99.0	-1.01	4.301	7.281
7,498.530	Fe I	32.0	-2.11	4.142	7.324
7,583.788	Fe I	142.0	-1.99	3.017	7.378
7,586.014	Fe I	150.0	-0.39	4.312	7.333
7,807.952	Fe I	84.0	-0.50	4.991	7.296
7,832.194	Fe I	161.0	-0.15	4.434	7.342
7,844.555	Fe I	17.0	-1.81	4.835	7.403
7,945.844	Fe I	189.0	0.15	4.386	7.318
7,998.939	Fe I	181.0	0.05	4.371	7.294
8,046.047	Fe I	170.0	-0.08	4.415	7.331
8,047.615	Fe I	125.0	-4.64	0.859	7.310
8,207.745	Fe I	90.0	-0.99	4.445	7.243
8,239.127	Fe I	93.0	-3.25	2.424	7.317
8,248.120	Fe I	92.0	-1.01	4.371	7.203
8,331.907	Fe I	161.0	-0.42	4.386	7.469
8,514.072	Fe I	193.0	-2.42	2.198	7.366
8,515.109	Fe I	132.0	-2.10	3.017	7.245
8,674.746	Fe I	182.0	-1.85	2.831	7.380
8,699.455	Fe I	91.0	-0.45	4.955	7.216
8,793.338	Fe I	150.0	-0.22	4.607	7.329
8,804.625	Fe I	111.0	-3.23	2.278	7.280
8,838.428	Fe I	169.0	-2.05	2.858	7.423
8,846.736	Fe I	68.0	-0.72	5.009	7.264
8,866.920	Fe I	175.0	-0.06	4.548	7.387
8,929.075	Fe I	60.0	-0.89	5.085	7.410
8,945.190	Fe I	103.0	-0.33	5.033	7.289
8,978.204	Fe I	17.5	-3.38	3.415	7.408
9,889.035	Fe I	103.0	-0.38	5.033	7.246
5,256.938	Fe II	77.0	-4.17	2.891	7.345
5,264.812	Fe II	119.0	-3.23	3.230	7.378
5,284.109	Fe II	143.0	-3.19	2.891	7.342
5,325.554	Fe II	115.0	-3.20	3.221	7.289
5,414.073	Fe II	96.0	-3.48	3.221	7.259
5,425.257	Fe II	115.0	-3.22	3.199	7.259
5,525.125	Fe II	53.0	-4.12	3.267	7.337
5,534.847	Fe II	146.0	-2.86	3.245	7.403
5,591.368	Fe II	23.0	-4.68	3.267	7.371

Table 1. Continued

Wavelength (angstroms)	Identification	Eq.Width (miliangstroms)	lggf	E_{low} (eV)	logN (logN(H)=12.00)
5,991.376	Fe II	99.0	-3.66	3.153	7.378
6,084.111	Fe II	76.0	-3.81	3.199	7.253
6,149.258	Fe II	102.0	-2.67	3.889	7.199
6,179.384	Fe II	11.5	-2.75	5.568	7.357
6,238.392	Fe II	121.0	-2.63	3.888	7.420
6,239.366	Fe II	31.0	-4.87	2.806	7.230
6,239.953	Fe II	56.0	-3.51	3.889	7.397
6,247.557	Fe II	140.0	-2.33	3.891	7.393
6,269.967	Fe II	26.0	-4.62	3.245	7.329
6,307.529	Fe II	7.5	-5.68	2.828	7.344
6,369.462	Fe II	71.0	-4.25	2.891	7.285
6,407.251	Fe II	60.0	-3.51	3.888	7.441
6,432.680	Fe II	111.0	-3.50	2.891	7.073
6,456.383	Fe II	160.0	-2.08	3.903	7.400
6,516.081	Fe II	148.0	-3.38	2.891	7.431
7,222.394	Fe II	79.0	-3.30	3.888	7.453
7,224.487	Fe II	78.0	-3.24	3.889	7.386
7,310.216	Fe II	54.0	-3.36	3.889	7.167
7,449.335	Fe II	75.0	-3.08	3.888	7.166
7,515.831	Fe II	51.0	-3.50	3.903	7.269
7,711.724	Fe II	131.0	-2.45	3.903	7.263
7,841.389	Fe II	18.0	-4.25	3.903	7.379

Table 2. Atmospheric parameters of HD204075

T_{eff} (K)	log *g*	[Fe/H]	Reference
5,196	1.60	-0.15	Sneden et al. (1981)
5,220	1.55	-0.45	McWilliam (1990)
5,209	2.14	-0.04	Antipova et al.(2004)
5,260	1.72	-0.19	Gopka et al. (2006)
5,250	1.53	-0.09	Smiljanicet et al. (2007)
5,220	1.55	-0.45	Cenarro et al. (2007)
5,397	1.48	-0.14	Prugniel et al. (2011)
5,428	2.37	+0.18	Luck (2014)
5,300	1.50	+0.06	de Castro et al. (2016)
5,300	1.82	-0.18	This paper

previously published abundances for this barium star and the second ionization potentials of corresponding elements. This comparison allows us to confirm or reject the existence of the influence of accretion of hydrogen and helium from the interstellar environment. Such accretion was discussed by Greenstein (1949), Bohm-Vitense (2006), and Yushchenko et al. (2015).

We adopted the abundances of chemical elements in the photosphere of HD204075 from Antipova et al. (2004) and Gopka et al. (2006) and plot these against the second ionization potentials of chemical elements (Fig. 2). No clear correlations were apparent in this plot.

A comparison Fig. 2 of this paper with Fig. 6 in Yushchenko et al. (2015) and also with Fig. 1 in Jeong et al. (2018), where similar dependencies were shown for δ Sct type star ρ Pup and barium type star ζ Cyg, respectively, demonstrates that the dependencies described in these two papers, are not found in the atmosphere of HD204075. The most important of these non-detected dependencies is the correlation of the abundance of chemical elements against the second ionization potentials of these elements having second ionization potentials between 13.6 and 24.6 eV (the ionization potentials of hydrogen and helium respectively).

Let us accept that the accretion of interstellar hydrogen and helium from the interstellar environment in the atmospheres of ρ Pup and ζ Cyg was responsible for the correlations of relative abundances versus second ionization potentials. These correlations were not detected in HD204075. Therefore, evidence of accretion of interstellar or circumstellar hydrogen and helium was not found in the atmosphere of HD204075 and, so, other physical effects must be responsible for the abundance anomalies in this star-namely for overabundances of s-process elements.

Fig. 2 from Gopka et al. (2006) shows the strong influence of the accretion of nuclear-processed matter from the former red giant companion (now a white dwarf) to the atmosphere of another binary component, a modern red giant. This process is the usual explanation for chemical anomalies in barium stars. The accretion from the former red giant clearly changes the surface chemical abundances of a modern red giant and in stars with radiative atmospheres, including red giant stars, these changes remain for long time.

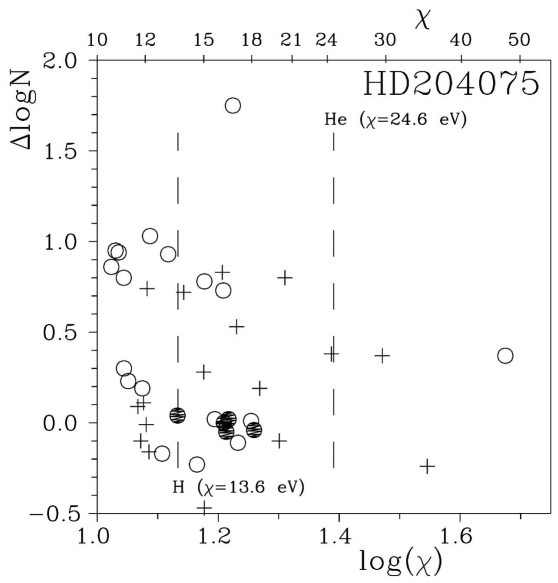

Fig. 2. A plot of relative surface abundances, calculated with respect to solar photosphere values, (ΔlogN) of chemical elements in HD204075 as a function of second ionization potentials (χ) of these elements. The abundances were taken from Antipova et al. (2004), and from Gopka et al. (2006) (circles and crosses respectively). The logarithms of ionization potentials are shown on the bottom part of the panel and the potentials themselves on the upper one. The filled circles are the abundances of Si, Ti, Cr, Fe, and Ni in accordance with Antipova et al. (2006). Jeong et al. (2018) used the abundances of these five chemical elements and also the abundance of aluminum for calculation of correlation coefficients, as described in the text. Vertical dashed lines mark the positions of the ionization energies of hydrogen and helium.

After the transition of a former red giant to a white dwarf, additional physical effects can be important for the production of chemical anomalies in other binary component, namely, modern red giant. One of these effects can be the accretion of hydrogen and helium from interstellar space. It is likely that the significance of this effect increases with time after the creation of a white dwarf companion. Jeong et al. (2018) determined the age dependence of the correlation of chemical abundances *versus* second ionization potentials in barium stars, as shown in the bottom panel of Fig. 4 in Jeong et al. (2018). Correlations were found for six chemical elements, namely, Al, Si, Ti, Cr, Fe, and Ni. Five of these elements (excluding Al) are marked in Fig. 2 of the current paper. Antipova et al. (2004) did not find the aluminum abundance; hence it is better to use the de Castro et al. (2016) survey, where the abundances of all six elements were found for HD204075.

The correlation coefficient of abundances of these elements (including Al) *versus* their second ionization potentials was 0.46±0.32 if we use the abundances calculated by de Castro et al. (2016). The age of HD204075 is $10^{7.8}$ years (de Castro et al. 2016). HD204075 is one of the youngest barium stars in the de Castro et al. (2016) survey. The age and correlation coefficient of HD204075 place it in the upper left corner of the bottom panel in Fig. 4 of Jeong et al. (2018) and corresponds to objects with minimum age and close to zero correlation coefficient of abundances *versus* second ionization potentials for the six chemical elements listed above. Taking into account the age of HD204075, the absence of evidence of hydrogen and helium accretion from interstellar medium, (Fig. 2), is therefore not surprising.

Havnes (1970, 1971) demonstrated that the accretion of hydrogen from interstellar medium can significantly change elemental abundances on stellar surfaces on the time scales of 10^8 years for hot stars with strong magnetic fields. Barium stars do not have strong magnetic fields and therefore the effects of hydrogen accretion should be important at longer time-scales. The bottom panel of Fig. 4 of Jeong et al. (2018) illustrates the possible influence of hydrogen accretion on the time scale from $10^{7.9}$ to $10^{9.6}$ years.

The young age of HD204075 can be confirmed by detection of technetium lines in the spectrum of its atmosphere (Gopka et al. 2006). Technetium (Tc) has no stable isotopes, the longest half-life is of the order of 10^5 years for Tc^{99}. Detection of this element confirms the recent transfer of nuclear processed matter from the evolved binary companion to the atmosphere of the modern red giant companion.

The main conclusion of this paper is that the accretion of hydrogen and helium atoms from the interstellar environment to the atmosphere of young barium star HD204075 produces no detectable anomalies of chemical composition over the past 10^5 to 10^8 years. For stars with weak magnetic fields, including HD204075, this type of accretion can be significant at time scales longer than 10^8 years.

This conclusion was not based on a detailed theory of hydrogen and helium accretion from interstellar medium to the atmospheres of normal stars with only a weak magnetic field, this theory, now only the hypothesis, should be developed in the future. Before doing so, however, it is necessary to collect observations which can be used to confirm or reject this hypothesis for different types of stars.

REFERENCES

Antipova LI, Boyarchuk AA, Pakhomov YV, Panchuk VE, analysis of atmospheric abundances in classical barium stars, Astron. rep. 48, 597-610 (2004). https://doi.org/10.1134/1.1777277

Asplund M, Grevesse N, Sauval AJ, Scott P, The chemical composition of the sun, Annu. Rev. Astron. Astrophys. 47, 481-522 (2009). https://doi.org/10.1146/annurev.

astro.46.060407.145222

Bagnulo S, Jehin E, Ledoux C, Cabanac R, Melo C, et al., ESO Paranal Science Operations Team, The UVES paranal observatory project: a library of high-resolution spectra of stars across the hertzsprung-russell diagram, The Messenger. 114, 10 (2003). https://www.eso.org/sci/publications/messenger/archive/no.114-dec03/messenger-no114-10-14.pdf

Biémont E, Palmeri P, Quinet P, D.R.E.A.M. database on rare Earths at Mons University (2002) [Internet], viewed 2017 Apr 14, available from: http://hosting.umons.ac.be/html/agif/databases/dream.html

Böhm-Vitense E, The puzzle of the metallic line stars, Publ. Astron. Soc. Pac. 118, 419-435 (2006). http://doi.org/10.1086/499385

Cenarro AJ, Peletier RF, Sánchez-Blázquez P, Salam SO, Toloba E, et al., Medium-resolution isaac newton telescope library of empirical spectra - II. The stellar atmospheric parameters, Mon. Not. R. Astron. Soc. 374, 664-690 (2007). http://doi.org/10.1111/j.1365-2966.2006.11196.x

de Castro DB, Pereira CB, Roig F, Jilinski E, Drake NA, et al., Chemical abundances and kinematics of barium stars, Mon. Not. R. Astron. Soc. 459, 4299-4324 (2016). http://doi.org/10.1093/mnras/stw815

Fuhr JR, Wiese WL, A critical compilation of atomic transition probabilities for neutral and singly ionized iron, J. Phys. Chem. Ref. Data 35, 1669-1809 (2006). http://doi.org/10.1063/1.2218876

Gopka V, Yushchenko A, Lambert D, Drake N, Rostopchin S, Heaviest s-process elements in the atmospheres of barium stars, in Proceedings of the International Symposium on Nuclear Astrophysics-Nuclei in the Cosmos - IX, Geneva, Switzerland, 25-30 Jun 2006. http://pos.sissa.it/archive/conferences/028/105/NIC-IX_105.pdf

Gopka VF, Yushchenko AV, Mishenina TV, Kim C, Musaev FA, et al., Atmospheric chemical composition of the halo star HD 221170 from a synthetic-spectrum analysis, Astron. Rep. 48, 577-587 (2004). http://doi.org/10.1134/1.1777275

Greenstein JL, Analysis of the metallic-line stars. II. Astrophys. J. 109, 121-138 (1949). http://doi.org/10.1086/145112

Havnes O, Abundances and acceleration mechanisms of cosmic rays, Nature, 229, 548-549 (1970). http://doi.org/10.1038/229548a0

Havnes O, Magnetic stars as generators of cosmic rays, Astron. Astrophys. 13, 52-57 (1971). http://adsabs.harvard.edu/abs/1971A%26A....13...52H

Havnes O, Conti PS, Magnetic accretion processes in peculiar a stars, Astron. Astrophys. 14, 1-11 (1971). http://adsabs.harvard.edu/abs/1971A%26A....14....1H

Hirata R, Horaguchi T, VizieR online data catalog: Atomic spectral line list, SIMBAD Catalog VI/69 (1995). http://vizier.cfa.harvard.edu/viz-bin/Cat?VI/69

Jeong Y, Yushchenko AV, Doikov DN, The interaction between accretion from the interstellar medium and accretion from the evolved binary component in barium stars, J. Astron. Space Sci. 35, 1-6 (2018). http://doi.org/10.5140/JASS.2017.35.1.1

Kang YW, Yushchenko A, Hong K, Kim S, Yushchenko V, Chemical composition of the components of eclipsing binary star ZZ bootis, Astron. J. 144, A35 (2012). http://doi.org/10.1088/0004-6256/144/2/35

Kang YW, Yushchenko AV, Hong K, Guinan EF, Gopka VF, Signs of accretion in the abundance patterns of the components of the RS CVn-type eclipsing binary star LX persei, Astron. J. 145, A167 (2013). http://doi.org/10.1088/0004-6256/145/6/167

Kurucz RL, SYNTHE spectrum synthesis programs and line data (Kurucz CD-ROM, Smithsonian Astrophysical Observatory, Cambridge, MA, 1993)

Luck RE, Parameters and abundances in luminous stars, Astron. J. 147, 137 (2014). http://doi.org/10.1088/0004-6256/147/6/137

McWilliam A, High-resolution spectroscopic survey of 671 GK giants. I-Stellar atmosphere parameters and abundances, Astrophys. J. Sppl. 74, 1075-1128 (1990). http://doi.org/10.1086/191527

Michaud G, Diffusion processes in peculiar a stars, Astrophys. J. 160, 641-658 (1970). http://doi.org/10.1086/150459

Morton DC, Atomic data for resonance absorption lines. II. Wavelengths longward of the lyman limit for heavy elements, Astrophys. J. Suppl. Ser. 130, 403-436 (2000). http://doi.org/10.1086/317349

Piskunov NE, Kupka F, Ryabchikova TA, Weiss WW, Jeffery CS, VALD: The vienna atomic line data base, Astron. Astrophys. Suppl. 112, 525-535 (1995). http://adsabs.harvard.edu/abs/1995A%26AS..112..525P

Proffitt CR, Michaud G. Abundance anomalies in A and B stars and the accretion of nuclear-processed material from supernovae and evolved giants, Astrophys. J. 345, 998-1007 (1989). http://doi.org/10.1086/167969

Prugniel Ph, Vauglin I, Koleva M, The atmospheric parameters and spectral interpolator for the MILES stars, Astron. Astrophys. 531, A165 (2011). http://doi.org/10.1051/0004-6361/201116769

Scott P, Asplund M, Grevesse N, Bergemann M, Sauval AJ, The elemental composition of the Sun. II. The iron group elements Sc to Ni, Astron. Astrophys. 573, 33(2015). http://doi.org/10.1051/0004-6361/201424110

Smiljanic R, Porto de Mello GF, da Silva L, Abundance analysis of barium and mild barium stars, Astron. Astrophys. 468, 679-

693 (2007). http://doi.org/10.1051/0004-6361:20065867

Sneden C, Lambert DL, Pilachowski CA, A study of CNO elements in barium stars, Astrophys. J. 247, 1052-1062 (1981). http://doi.org/10.1086/159114

Yushchenko AV, URAN: A Software System for the Analysis of Stellar Spectra, in Proceedings of the 20th Stellar Conference of the Czech and Slovak Astronomical Institutes, Brno, Czech Republic, 5–7 Nov 1997.http://adsabs.harvard.edu/abs/1998vsr..conf..201Y

Yushchenko AV, Gopka VF, Kang YW, Kim C, Lee BC, et al., The chemical composition of ρ puppis and the signs of accretion in the atmospheres of B-F-type stars, Astron. J. 149, A59 (2015). http://doi.org/10.1088/0004-6256/149/2/59

Yushchenko AV, Gopka VF, Khokhlova VL, Musaev FA, Bikmaev IF, Atmospheric chemical composition of the "twin" components of equal mass in the CP SB2 system 66 Eri, Astron. Lett. 25, 453-466 (1999). http://adsabs.harvard.edu/abs/1999AstL...25..453Y